Journal of Engineering Mathematics, Vol. 8, No. 2, April 1974
Noordhoff International Publishing–Leyden
Printed in The Netherlands

Singularities of viscous flow

Part II: Applications to slender body theory

J. R. BLAKE*

Engineering Science Department, California Institute of Technology, Pasadena, California, USA

(Received July 24, 1973 and in revised form November 2, 1973)

SUMMARY

The force and torque on a slender body in Stokes flow is obtained by using a distribution of singularities along the centreline and the required image system to satisfy the no-slip condition and the plane boundary. It is found that the force on a slender body increases rapidly as it approaches within a body length of the boundary, but not the torque. To rule out "wall effects", experiments on slender bodies, such as flagellated or ciliated micro-organisms, should be carried out a distance of many body lengths (not radii!) from all boundaries. The ratio of normal to tangential resistance coefficients is found to be greater than 2 (the maximum in an infinite fluid) in the presence of walls.

1. Introduction

In the companion paper (Part I) to this, the fundamental singularities of viscous flow and their image system in the presence of a no-slip boundary are discussed. In this paper, applications of these singularities in the form of calculating the drag or torque of a slender body in the presence of a stationary boundary are obtained.

For smooth rigid slender bodies, the distribution of viscous fluid singularities ("stokeslets") along the centreline has produced relatively accurate calculations for both the force distribution and the drag (Burgers [3]; Tuck [15], [16]; Tillett [14]; Batchelor [1]; Cox [7]) although the usual end condition difficulties of slender body theory arise. For twisted or helical rigid slender bodies inaccuracies in the strength of the centreline distribution of singularities and the drag have been found (Clarke [6], Chwang and Wu [5]) and either a surface distribution or an improved coordinate system is needed to improve the accuracy. Hancock [10] used a centreline distribution of stokeslets and source-doublets along a flexible cylinder to represent the movement of flagellated micro-organisms. Very few attempts have been made to model flexible or curved slender bodies with the exception of Hancock [10] and Cox [7].

Biological fluid mechanics encourages us to re-evaluate the previous studies, and even initiate new ones; this being particularly so in the case of the mechanics of micro-organism propulsion. Many flagellated bacteria propel themselves by propagation of helical waves along their tails, which induces a torque on both the head (if it has one) and the tail, hence inducing a rotational movement of the bacterium relative to the fluid at infinity (or the laboratory frame). This is brought about by the necessity to balance both the linear and angular momentum. Because of this simple fact, Chwang and Wu [4] supplemented the usual "stokeslets" distribution (corresponding to force) along the centreline with a "rotlet" (corresponding to a torque) distribution. In this paper, we will discuss the torque induced on a rotating slender body in both an infinite (§3) and semi-infinite viscous fluid (§5). We should also point out that the propagation of helical waves along a flagellum poses other problems which can be labelled the "neighbouring" and "end" effects. The "neighbouring" effect is concerned with the influence of nearby sections of a slender body when we have some "coiling up" of the body and also the effect of the relative motion of one section to another (i.e. they are moving at different velocities). "End effects" are considered with the influence of differing end shapes on both "stokeslets" and "rotlet" singularity distributions. Both of these effects will not be discussed in any detail in this paper.

* Present address: Department of Applied Mathematics and Theoretical Physics, Silver St., Cambridge, England.

Another problem which arises in the study of micro-organism propulsion is with regard to the influence of walls or bounding surfaces, such as a slide or coverslip, may have on their observed motion: "Are the observed planar beating patterns of many protozoa an artifact induced by the influence of either slide or coverslip?" This is a question we cannot answer with any degree of certainty at present, but the present study (§4, 5) does investigate the effects of a wall on both a rotating and translating rigid slender body. The experimental study of Winet [17] on the wall effect on ciliated micro-organisms will undoubtedly be of considerable interest to the theoretician. This study will also be helpful in understanding the complex movements of cilia on many protozoa. Cilia, like flagella, are long slender organelles, but in this case a very large number of them (10^{4-6}) are attached to the outer surface of a much larger organism (cilia O (10 μm), organism e.g. *Opalina* 300 μm, *Paramecium* 250 μm).

In the next section, we will discuss some basic fundamentals which have been used to date in calculating the force distribution and the velocity of propulsion of both flagellated and ciliated micro-organisms and indicate the improvements we feel are necessary. This has been called the "Gray and Hancock theory" after the paper by Gray and Hancock [9], inspired by the original Hancock [10] paper.

2. Gray and Hancock theory

Gray and Hancock's [9] paper used the concept of Taylor's [13] coefficients of resistance for an infinite cylinder in a viscous fluid. That is, for a flexible body it was supposed that each section of the elongated body exerted the same force as an infinite cylinder moving with the same velocity, direction and waveform. At low Reynolds number the force exerted on each element of the cylinder is proportional to the local velocity. The movement of each portion of the cylinder can be described in terms of two components of velocity, one normal (V_N) to the cylinder and the other tangential (V_T) to it. The coefficients of resistance C_N and C_T are defined as the dimensional constant which give the relationship between both the normal δF_N and tangential δF_T force elements and V_N and V_T respectively on an element of cylinder δs in length. Thus,

$$\delta F_N = C_N V_N \delta s\,, \quad \delta F_T = C_T V_T \delta s\,. \tag{1}$$

Gray and Hancock [9] obtained the following relationship between the normal and tangential coefficients of resistance,

$$C_N = 2C_T\,, \quad C_T = \frac{2\pi\mu}{\log(2\lambda/r_0) - \frac{1}{2}}, \tag{2}$$

where μ is the viscosity, λ is the wavelength and r_0 is the radius of the flexible cylinder.

If we represent the centreline of a slender body in an infinite fluid in cartesian coordinates by $\xi(s, t)$ where s is the arc length along the slender body and t is time then,

$$V_T = (\boldsymbol{v}\cdot\boldsymbol{t})\,, \quad V_N = (\boldsymbol{v}\cdot\boldsymbol{n})\,,$$

where

$$\boldsymbol{v} = \frac{\partial \xi}{\partial t} - \boldsymbol{U}\,, \tag{3}$$

$\boldsymbol{t}$ is the tangent, $\boldsymbol{n}$ the normal to the slender body while $\boldsymbol{U}$ is the velocity of the organism relative to the fluid at infinity. Similarly, we can express $\delta \boldsymbol{F}$ in terms of both δF_T and δF_N as,

$$\delta \boldsymbol{F} = \delta F_T \boldsymbol{t} + \delta F_N \boldsymbol{n} = C_T((\boldsymbol{v}\cdot\boldsymbol{t})\boldsymbol{t} + 2(\boldsymbol{v}\cdot\boldsymbol{n})\boldsymbol{n})\delta s \tag{4}$$

Now $\boldsymbol{t} = \partial\boldsymbol{\xi}/\partial s$ and $I = \boldsymbol{nn} + \boldsymbol{bb} + \boldsymbol{tt}\,(\boldsymbol{v}\cdot\boldsymbol{b} = 0)$ is the idemfactor so we can write (4) as

$$\delta F_i = C_T\left(2\delta_{ij} - \frac{\partial \xi_i}{\partial s}\frac{\partial \xi_j}{\partial s}\right) v_j \delta s\,. \tag{5}$$

This is exactly the expression for the force distribution along a slender body obtained by Cox [7] in his rigorous matched asymptotic expansion approach. The force exerted over the whole elongated body can be obtained by integration.

3. Torque on a slender body: infinite viscous fluid

In cartesian coordinates, the velocity field due to a rotlet of strength $\boldsymbol{M}$ is represented by the following equation

$$\boldsymbol{u} = \frac{\boldsymbol{M} \wedge \boldsymbol{x}}{8\pi\mu|\boldsymbol{x}|^3}, \quad p = \text{const.} \tag{6}$$

If we consider a distribution $M_0(s)$ of singularities along the centreline of an axisymmetric slender body of radius $r_0(x_1)$, $|x_1| \leqslant l$ which is rotating with an angular velocity ω then the integral equation to be satisfied in cylindrical coordinates is the following:

$$\omega r_0(x_1) = \frac{1}{8\pi\mu}\int_{-l}^{l} \frac{M_0(s) r_0(x_1)\,ds}{((x_1-s)^2+r_0^2(x_1))^{\frac{1}{2}}}. \tag{7}$$

This equation has been solved exactly by Chwang and Wu [5] for a class of axisymmetric bodies ranging from a sphere to a very slender body. Here, though, we will only discuss the limiting case of their results for a very slender body. Following the philosophy of Batchelor [1], we will assume that $M_0(x_1)$ is approximately constant along most of the slender body, except possibly the ends. Thus

$$\omega \sim \frac{M_0(x_1)}{8\pi\mu}\int_{-l}^{l} \frac{ds}{((x_1-s)^2+r_0^2)^{\frac{1}{2}}}. \tag{8}$$

This first approximation to the torque strength $M_0(x_1)$ yields,

$$M_0(x_1) = 4\pi\mu\omega r_0^2(x_1). \tag{9}$$

Actually, we can derive (9) more rigorously than the above method if we integrate (7) by parts, obtaining

$$8\pi\mu\omega = \left[\frac{-M_0(s)(x_1-s)}{r_0^2((x_1-s)^2+r_0^2)^{\frac{1}{2}}}\right]_{-l}^{l} + \frac{1}{r_0^2}\int_{-l}^{l} \frac{M_0'(s)(x_1-s)}{((x_1-s)^2-r_0^2)^{\frac{1}{2}}}\,ds. \tag{10}$$

Now we may approximate the kernel part of the integral in (10) by $\operatorname{sgn}(x_1-s)$, so we obtain the following on assuming symmetry in $M(s)$ (i.e. $M(l)=M(-l)$)

$$8\pi\mu\omega \sim \frac{2M_0(x_1)}{r_0^2} + \frac{M_0(l)}{r_0^2}\left[\frac{l-x_1}{((l-x_1)^2+r_0^2)^{\frac{1}{2}}} + \frac{l+x_1}{((l+x_1)^2+r_0^2)^{\frac{1}{2}}} - 2\right]. \tag{11}$$

In the middle section of the slender body, the coefficient of $M(l)$ is approximately zero, so we reproduce (9) for the strength of $M_0(x_1)$ while at the ends

$$M_0(l) \sim 8\pi\mu\omega r_0^2 \tag{12}$$

which is exactly twice the strength in the middle section.

The result quoted in (9) agrees with that obtained by Lamb [11] for the torque/unit length of an infinitely long cylinder. Because many flagellated micro-organisms both translate and rotate, it was found to be necessary to supplement the force coefficients defined in (2) with the torque coefficient C_M, defined as

$$C_M = 4\pi\mu r_0^2, \qquad \delta T = C_M \omega\,\delta s \tag{13}$$

for us to balance both linear and angular momentum.

4. Force on a translating slender body: semi-infinite fluid

Considerable attention has been given in recent years to the calculation of the force distribution

along a slender body in an infinite viscous fluid (Batchelor [1]; Tillett [14]; Cox [7]; Clarke [6]). In this section we will consider the influence of a stationary no-slip boundary on this force distribution along the centreline of a slender body of length $2l$ and radius $r_0(x_1)$ where $|x_1| < l$ which is situated a distance h above the no-slip boundary $x_3 = 0$ (see Fig. 1). We will suppose the distribution is parallel to the x_1-axis. A similar method to this has recently been used by de Mestre [8], when he uses Lorentz's [12] image reflection technique, but here we start immediately with the correct Green's function.

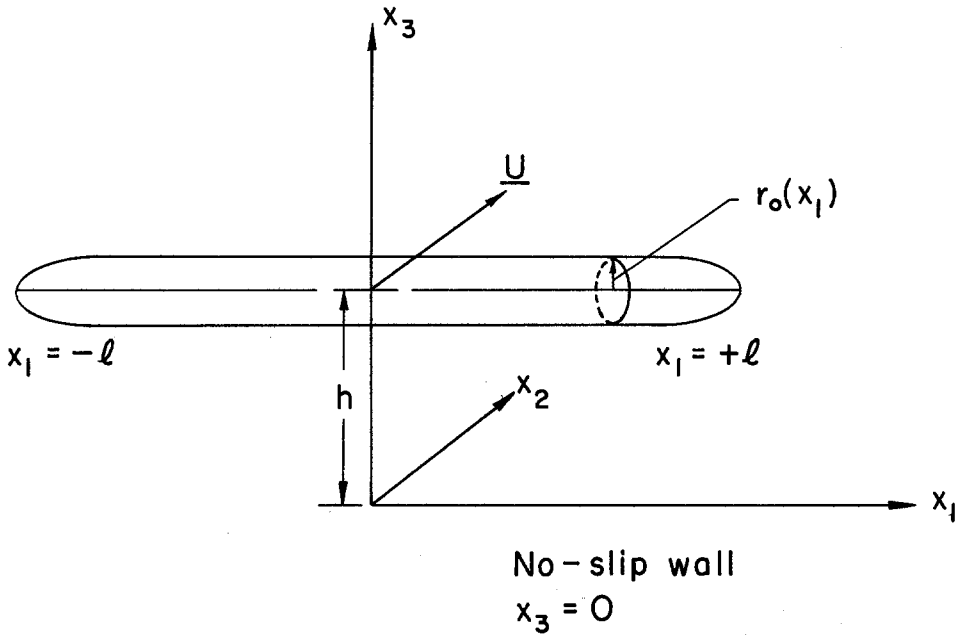

Figure 1. Illustrates the geometry of the slender body relative to the cartesian coordinate system fixed in the wall.

The singularity of most importance at low Reynolds number is the stokeslet distribution, since it is the fundamental singularities of stokes flow. For a slender body the distribution strength of all the other singularities is at most $O(r_0 F)$, which in the ordering of this problem proves to be a lower order of magnitude approximation. This is apparent if we go from the unique and exact surface distribution of stokeslets by Taylor series to a line distribution of many singularities. If we considered a source-doublet distribution, by extension of the result for a sphere obtained by Stokes, this would have an order of magnitude of $O(r_0^2 F)$. Thus all the essential features of this problem for a slender body can be obtained by considering a "stokeslet" and its image distribution alone.

In this problem, we define two small non-dimensional parameters ε_l and ε_h as follows,
Define

$$R = \operatorname*{Max}_{x_1 \in [-l, l]} r_0(x_1),$$

then

$$\varepsilon_l = \frac{R}{l} \ll 1, \quad \varepsilon_h = \frac{R}{h} \ll 1 \tag{14}$$

where h is the height above the wall. With the constraint that $\varepsilon_h \ll 1$, we can formally write down the integral equations using a centreline distribution as follows,

$$u_i(\boldsymbol{x}) = \int_{-l}^{l} G_{ij}(\boldsymbol{x}, s) F_j(s) ds, \quad p(\boldsymbol{x}) = \int_{-l}^{l} P_j(\boldsymbol{x}, s) F_j(s) ds \tag{15a}$$

where

$$G_{ij}(\boldsymbol{x}, s) = \frac{1}{8\pi\mu}\left[\left(\frac{\delta_{ij}}{r} + \frac{r_i r_j}{r^3}\right) - \left(\frac{\delta_{ij}}{R} + \frac{R_i R_j}{R^3}\right)\right.$$
$$\left. + 2h(\delta_{j\alpha}\delta_{\alpha k} - \delta_{j3}\delta_{3k})\frac{\partial}{\partial R_k}\left(\frac{hR_i}{R^3} - \left(\frac{\delta_{i3}}{R} + \frac{R_i R_3}{R^3}\right)\right)\right], \quad \alpha = 1, 2 \tag{15b}$$

and

$$P_j(\boldsymbol{x}, s) = \frac{1}{4\pi}\left[\frac{r_j}{r^3} - \frac{R_j}{R^3} - 2h(\delta_{j\alpha}\delta_{\alpha k} - \delta_{j3}\delta_{3k})\frac{\partial(R_3/R^3)}{\partial R_k}\right] \tag{15c}$$

where

$$r = [(x_1 - s)^2 + x_2^2 + (x_3 - h)^2]^{\frac{1}{2}}$$
and
$$R = [(x_1 - s)^2 + x_2^2 + (x_3 + h)^2]^{\frac{1}{2}} \tag{15d}$$

with the components of r and R being obvious from this definition. The boundary conditions to be applied at the surface of the slender body are,

$$\boldsymbol{u} = \boldsymbol{U} \text{ on } r = r_0(x_1). \tag{16}$$

We will use two approaches to solving the integral equations (15a, b, c, d) with boundary conditions as stated in (16), one being an asymptotic expansion for the force, the other being a direct numerical assault on the integral equations using a matrix inversion technique.

4.1. *Asymptotic expansion*

The singular part of the integral equations (15a, b) have been looked at in considerable detail, since they represent the motion of a slender body in an infinite fluid, but for thoroughness we will repeat the approximations here. Thus we have to solve, or approximate, the following integral given the stokeslet distribution is along the centreline of a slender body, that is

$$u_i(\boldsymbol{x}) = \frac{1}{8\pi\mu}\int_{-l}^{l}\left(\frac{\delta_{ij}}{r} + \frac{r_i r_j}{r^3}\right)F_j(s)\,ds \tag{17a}$$

where $r = ((x_1 - s)^2 + x_2^2 + x_3^2)^{\frac{1}{2}}$ with the components being obvious from this definition. We wish to evaluate the integral (17a) on the surface of the slender body, which in the local cylindrical coordinates of the body is $(x_1, r_0(x_1), \theta)$. Note the boundary condition to be applied on the surface defined in (16) is for the complete integral equation defined in (15a, b, c, d). Since (17a) is singular in the limit as $r_0(x_1)$ tends to zero we can conclude that the major contribution from the integral (17a) comes from the vicinity of the point $s = x_1$. Thus the analysis is simplified if we reorganise the integral as follows

$$u_i(x_1, \theta) = \frac{F_j(x_1)}{8\pi\mu}\int_{-l}^{l}\left(\frac{\delta_{ij}}{r} + \frac{r_i r_j}{r^3}\right)ds$$
$$+ \frac{1}{8\pi\mu}\int_{-l}^{l}\left(\frac{\delta_{ij}}{r} + \frac{r_i r_j}{r^3}\right)(F_j(s) - F_j(x_1))\,ds, \tag{17b}$$

where $r = [(x_1 - s)^2 + r_0^2(x_1)]^{\frac{1}{2}}$.

In Table 1 the values of the integral,

$$I_{ij} = \int_{-l}^{l}\left(\frac{\delta_{ij}}{r} + \frac{r_i r_j}{r^3}\right)ds \tag{17c}$$

after applying the slenderness limits, to functions, such as

$$\sinh^{-1}((x_1 - s)/r_0) \sim \log(2(x_1 - s)/r_0),$$

are listed.

TABLE 1

Approximate values of I_{ij} on application of the slenderness property

I_{ij}	I_{11}	$I_{12}=I_{21}$	I_{22}	$I_{23}=I_{32}$	$I_{13}=I_{31}$	I_{33}
Approximate	$2\log\frac{4(l^2-x_1^2)}{r_0^2}$	0	$\log\frac{4(l^2-x_1^2)}{r_0^2}$	$\sin 2\theta$	0	$\log\frac{4(l^2-x_1^2)}{r_0^2}$
values	-2		$+1+\cos 2\theta$			$+1-\cos 2\theta$

The term in $\cos 2\theta$ and $\sin 2\theta$ can be removed either by taking an average in θ around the slender body, or the same effect can be obtained by using a distribution of potential source doublets along the centre-line of the slender body. The important point to note is that these terms correspond to higher order approximations of the integral equation and can, to this order at any rate, be neglected. The second part of the integral in (17b) is equal to

$$\frac{1}{8\pi\mu}(\delta_{ij}+\delta_{i1}\delta_{j1})\int_{-l}^{l}\frac{F_j(s)-F_j(x_1)}{|s-x_1|}\,ds+E \tag{17d}$$

where

$$E=\begin{cases} O(\varepsilon_l^2\log\varepsilon_l,\ \varepsilon_l^2)\dfrac{F}{\mu_l}\ ;\ \text{if } F_j(x_1)\in C^\infty \\ O(\varepsilon_l^{\frac{1}{2}})\dfrac{F}{\mu_l}\ \text{if } F_j(x_1)\in L^2 \end{cases} \tag{17e}$$

where C^∞ is the space of infinitely differentiable continuous functions and L_2 is the space of square integrable functions. The stronger error terms follow immediately from the neglected term in the asymptotic expansion (see Tuck [16]). The weaker error term can be derived by splitting the integral into three parts, that is by considering two non-singular parts and a region around the singular zone. The "slender body equations" quoted in (17c, d) can be obtained from Tuck [16] and Batchelor [1].

Thus with the rearrangement of the I_{ij} terms by splitting the log term into two parts we obtain the following approximation at the surface of the slender body. Since $\varepsilon_h \ll 1$ we may leave the "wall effect" in the form of an integral. Thus we obtain

$$\begin{aligned} u_i=\frac{1}{4\pi\mu}\Bigg[&\left(\log\frac{2l}{R}+\log\left(\frac{(1-(x_1/l)^2)^{\frac{1}{2}}}{r_0(x_1)/R}\right)^*\right)(F_i+\delta_{i1}F_1)\\ &+(\tfrac{1}{2}\delta_{ij}-\tfrac{3}{2}\delta_{i1}\delta_{j1})F_j\Bigg]\\ &+\frac{1}{8\pi\mu}(\delta_{ij}+\delta_{i1}\delta_{j1})\int_{-l}^{l}\frac{F_j(s)-F_j(x_1)}{|s-x_1|}\,ds-W_i[F_j]+E \end{aligned} \tag{17f}$$

where the wall effect term is defined as follows

$$\begin{aligned} W_i[F_j]=\int_{-l}^{l}F_j(s)\Bigg[&\frac{\delta_{ij}}{R}+\frac{R_iR_j}{R^3}\\ &-2h(\delta_{j\alpha}\delta_{\alpha k}-\delta_{j3}\delta_{3k})\frac{\partial}{\partial R_k}\left(\frac{hR_j}{R^3}-\left(\frac{\delta_{i3}}{R}+\frac{R_iR_3}{R^3}\right)\right)\Bigg]\,ds\,. \end{aligned} \tag{17g}$$

This is essentially a "strong expansion" in that the error terms are algebraic. However, these equations (17f) prove difficult to solve and Tillett [14], Batchelor [1] and Cox [7] proposed a "weak asymptotic" expansion in powers of $(\log(2l/R))^{-1}$ because of the predominant term in (17f). We will use their approach in this section and define

$$F_i(x_1)=\sum_{n=1}^{\infty}F_i^{(n)}(x_1)\left(\log\frac{2l}{R}\right)^{-n}. \tag{18}$$

In theory this expansion needs to be completely evaluated before we need to improve the "strong expansion" in (17f). However in practice for finite ε_l we need only go to the mth term when $(\log(2/\varepsilon_l))^{-m} = O(\varepsilon_l^2)$.

On substitution into (17f) (the weak expansion) produces the following as a first approximation

$$F_i^{(1)} = 2\pi\mu U_j(2\delta_{ij} - \delta_{i1}\delta_{j1}) . \tag{19a}$$

We substitute this back into (17f) to obtain the second approximation, that is

$$F_i^{(2)} + \delta_{i1}F_1^{(2)} = -4\pi\mu\left[U_i \log\left(\frac{(1-(x_1/l)^2)^{\frac{1}{2}}}{r_0(x_1)/R}\right)^* + (\tfrac{1}{2}\delta_{ij} - \delta_{i1}\delta_{j1})U_j\right] + W_i[F_j^{(1)}] . \tag{19b}$$

The "wall effect" term may be evaluated analytically, but the algebra is far too lengthy to include in this paper. We shall, however, evaluate the second approximation numerically, making use of the non-dimensional clearance parameter δ, defined as follows,

$$\delta = \frac{h}{l} = \frac{\varepsilon_l}{\varepsilon_h} \tag{20}$$

In the following calculations, we have replaced the singular log term (*) from (19b) with the original $\sinh^{-1}$ function.

$$\log\left(\frac{(1-(x_1/l)^2)^{\frac{1}{2}}}{r_0(x_1)/R}\right)^* \doteqdot \tfrac{1}{2}\log\tfrac{1}{2}\left[1 - \frac{x_1}{l} + \left(\left(\frac{r_0(x_1)}{l}\right)^2 + \left(1 - \frac{x_1}{l}\right)^2\right)^{\frac{1}{2}}\right]$$
$$+ \tfrac{1}{2}\log\tfrac{1}{2}\left[1 + \frac{x_1}{l} + \left(\left(\frac{r_0(x_1)}{l}\right)^2 + \left(1 + \frac{x_1}{l}\right)^2\right)^{\frac{1}{2}}\right] - \log\frac{r_0(x_1)}{R}$$

The calculations were carried out for both a circular cylinder and a spheroid; the results can be seen in the following figures, the force components being non-dimensionalised with respect to the first approximation.

For most of the figures, we have taken $\varepsilon_l = 0.02$, other values of ε_l behave similarly providing the restriction $\varepsilon_l \ll 1$ is maintained. In Fig. 2, the force distribution per unit length is shown for a circular cylinder for different non-dimensional clearance values of δ. There is an increase

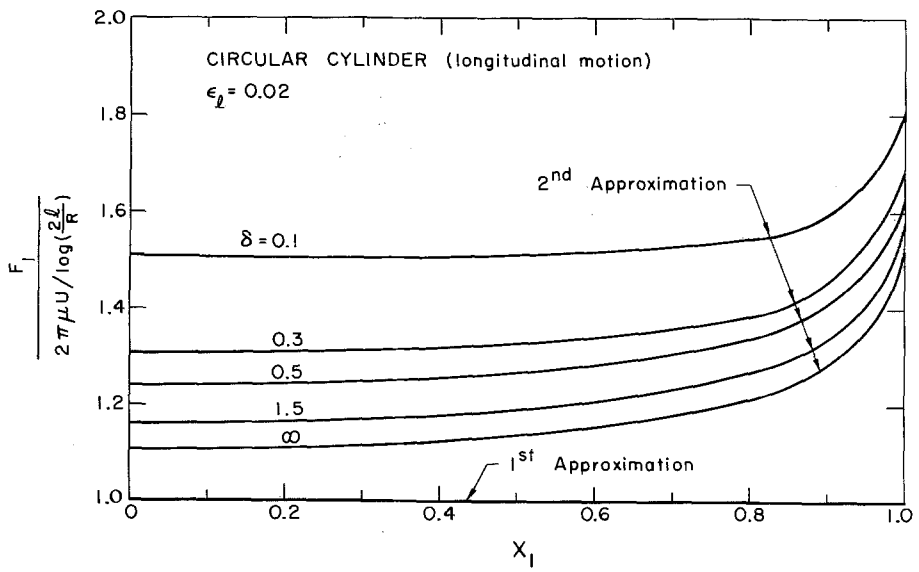

Figure 2. The second approximation for force distribution along a circular cylinder ($\varepsilon_l = 0.02$) for longitudinal motion, non-dimensionalised with respect to the first approximation. The distribution is symmetric around the central point so only half the distribution is shown.

of almost 40% in the resistance distribution for $\delta = 0.1$ over that in an infinite fluid (i.e. $\delta = \infty$). However, as δ increases, the force distribution slowly tends to that in an infinite fluid. Because we are using a circular cylinder, we have a discontinuity in slope at the ends so the force distribution tends to indicate a singular nature at these points. A surface distribution of singularities could probably remedy these problems at the ends.

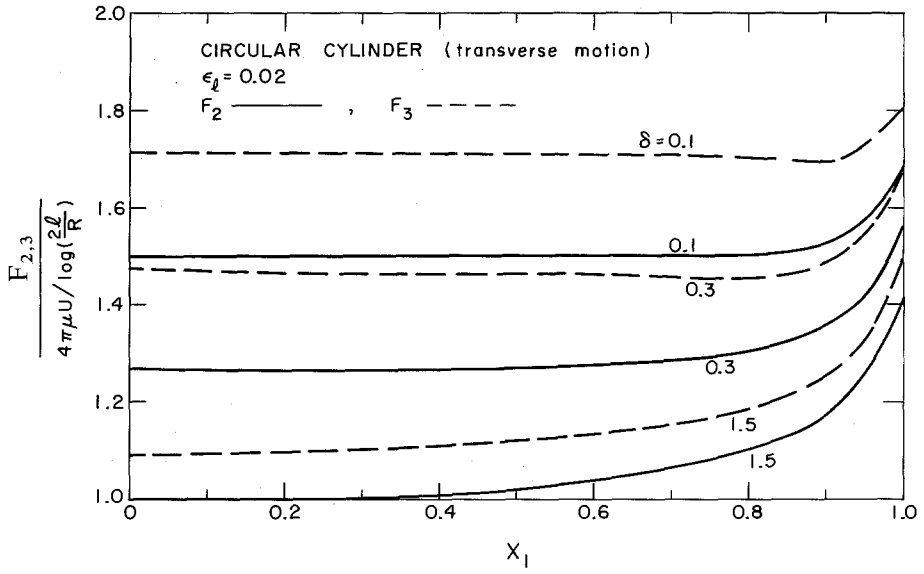

Figure 3. The second approximation to the force distribution along a circular cylinder ($\varepsilon_l = 0.02$) for transverse motions.

In Fig. 3, the force distribution for transverse motions are shown. In this case, though, there are two cases, movement parallel to the wall (F_2) and perpendicular to the wall (F_3). The significant result is that the theory predicts the resistance on a slender body moving towards the wall (i.e. F_3) is around 15% higher than motion parallel to the wall for $\delta = 0.1$ and 0.3 (also see discussion in exact numerical solutions). As we move further away from the wall, the discrepancy becomes less and eventually become the same when the fluid is effectively infinite. We may have anticipated this result qualitatively from the approximate solution for a sphere near a wall as the correction factor for the drag for motion parallel to the wall is $\frac{9}{16}a/h$ and $\frac{9}{8}a/h$ for motion perpendicular to the wall (a = radius sphere, h height above wall and $a/h \ll 1$). Another feature of the graphs is that they are almost constant for small values of δ, except near the ends. That is in the middle section the drag on the cylinder is similar to that on an infinite cylinder, or alternatively we could say that the interaction effects with the wall is the dominant feature of its motion.

In Fig. 4, we have plotted the ratio of the normal to tangential resistance coefficients for the two cases. We define

$$\gamma_1 = \frac{F_2/U_2}{F_1/U_1} \quad \text{and} \quad \gamma_2 = \frac{F_3/U_3}{F_1/U_1}. \tag{22}$$

We obtain the surprising result that the ratio γ can be greater than two when we include wall effects. In the middle section for $\delta = 0.1$, we obtain values around 2.3, but near the ends it decreases to values around 2.0. For a slender body in an infinite fluid, the ratio is always less than 2, approaching 2 asymptotically in the limit as ε_l tends to zero. deMestre [8] in his paper remarked that this ratio still held even when boundaries are included, but this paper indicates otherwise.

Fig. 5 indicates the variation of total drag as a function of the non-dimensional clearance δ for longitudinal motion. Plots are made for several values of ε_l. The graphs indicate that for

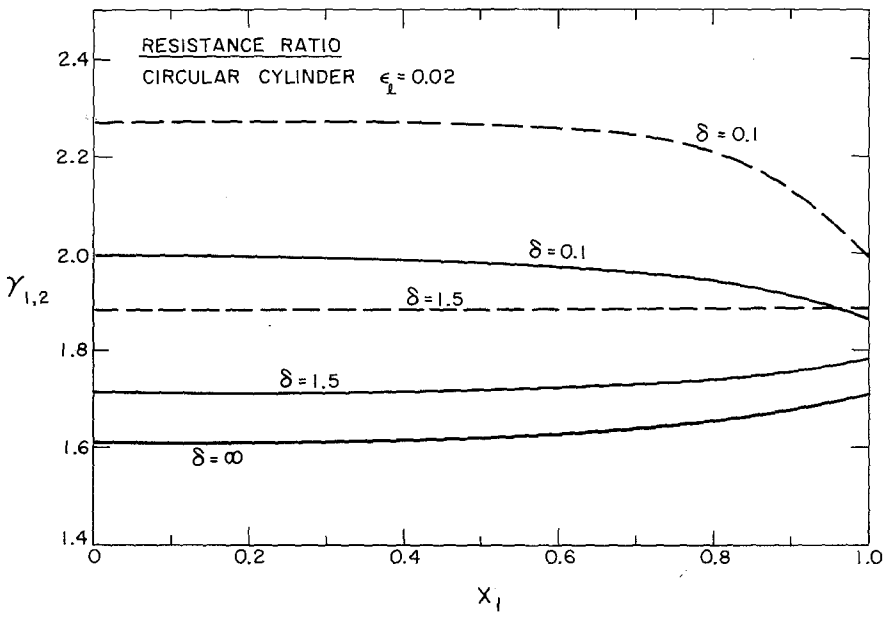

Figure 4. Ratio of resistance coefficients obtained from Figs. 3 and 4. γ_1 (——) and γ_2 (– – –) are defined in the text.

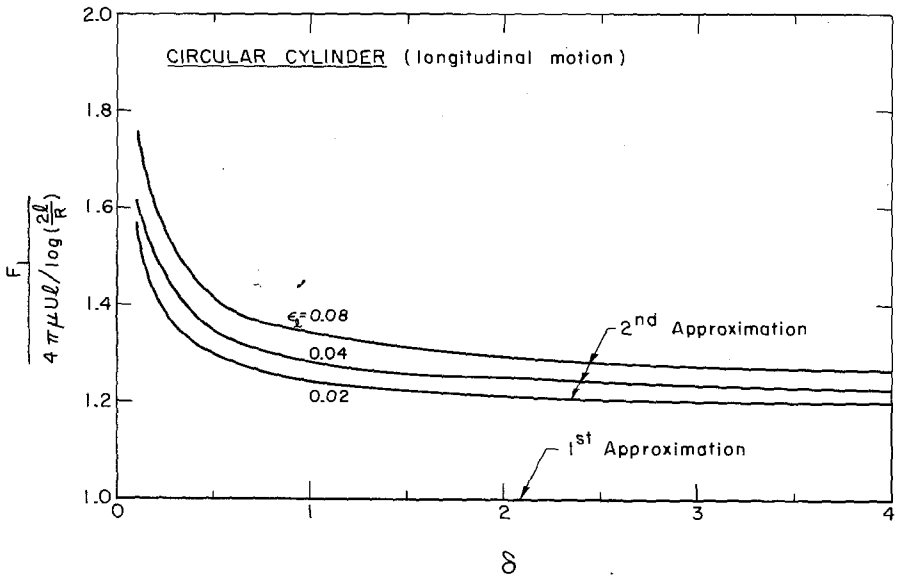

Figure 5. Variation of the second order non-dimensionalised total drag with respect to the clearance δ of the circular cylinder from the wall. Graphs for different values of ε_l are marked on the diagram.

values of δ less than one, the drag increases rapidly. This indicates that to minimize wall effects on slender bodies, we should be many body lengths (not radii!) away from the nearest boundary.

Calculations on a slender spheroid yields qualitatively similar features to that for a cylinder, except near the ends where we have a smoother profile.

4.2. *Direct numerical evaluation*

In this section, we will briefly discuss a direct numerical approach to solving (15a, b, c, d) for the force E boundary conditions (16). Thus, all we have to do is solve the matrix equation

$$\mathbf{G} \cdot \boldsymbol{F} = \boldsymbol{U} \tag{23}$$

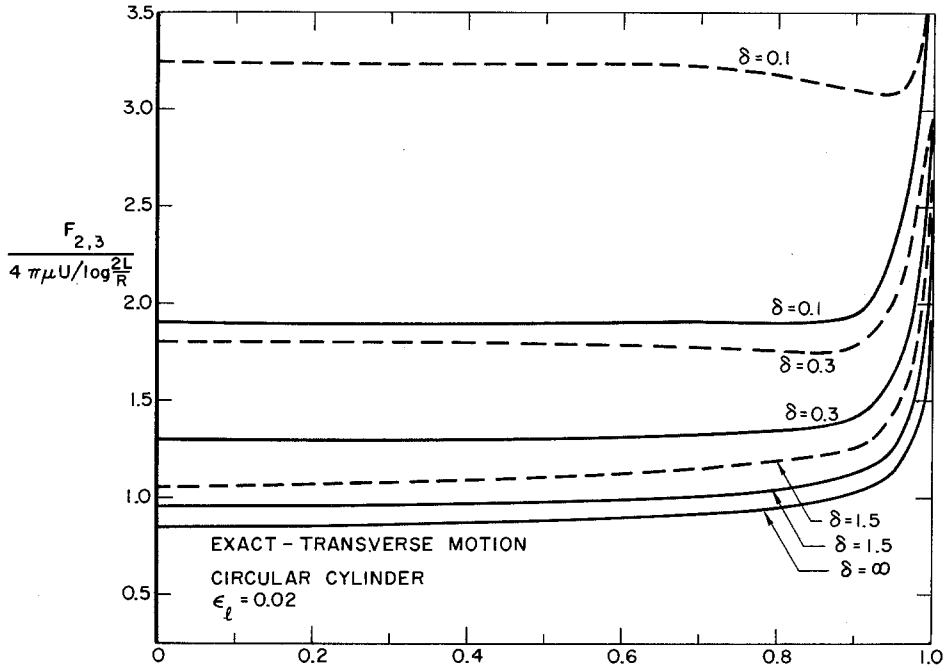

Figure 6. Graphs showing the numerical solutions of the force distribution for a circular cylinder in transverse motion ($\varepsilon_l = 0.02$) for various values of the clearance δ.

where **G** is the matrix defined by the kernel or Greens function defined in (15b), $\boldsymbol{F}$ is the unknown force distribution and $\boldsymbol{U}$ is the velocity vector. In the numerical work, care needs to be taken of the singular parts of the integral (i.e. $\varepsilon_l \to 0$).

In Fig. 6, the results from the direct numerical calculations are shown for transverse motions alone. The important feature to observe is that the numerical results predict a much larger resistance for $\delta = 0.1$ than does the asymptotic expansion approach (see Fig. 3). For larger values of δ they predict the same results (see e.g. $\delta = 1.5$). The singular nature at the ends is also more apparent when we use the numerical approach. Values of $\gamma_{1,2}$ in the numerical case approaches values around 3 for $\delta = 0.1$. This indicates that the asymptotic expansion is a poor one when δ becomes small, a more appropriate expansion in cases like this would be,

$$F_i(x_1) = \sum_{n=1}^{\infty} F_i^{(n)}(x_1) \left(\log \frac{2h}{R}\right)^{-n}, \tag{24}$$

that is the length scale is replaced by h.

5. Torque on a rotating slender body: semi-infinite fluid

The velocity and pressure field due to a distribution of "rotlets" along the centreline of a slender body and the corresponding image system due to the presence of a stationary plane boundary is as follows,

$$u_i(\boldsymbol{x}) = \int_{-l}^{l} G_{ij}^*(\boldsymbol{x}, s) M_j(s) ds$$

and (25a)

$$p(\boldsymbol{x}) = \int_{-l}^{l} P_j^*(\boldsymbol{x}, s) M_j(s) ds$$

where

$$G_{ij}^* = \frac{1}{8\pi\mu}\left[\frac{\varepsilon_{ijk} r_k}{r^3} - \frac{\varepsilon_{ijk} R_k}{R^3} + 2h\varepsilon_{kj3}\left(\frac{\delta_{ik}}{R^3} - \frac{3R_i R_k}{R^5}\right) + 6\varepsilon_{kj3}\frac{R_i R_k R_3}{R^5}\right] \tag{25b}$$

and

$$P_j^* = -\frac{1}{2\pi}\frac{\partial}{\partial R_k}\left(\frac{\varepsilon_{kj3}R_3}{R^3}\right)$$

where both r and R are defined previously. Here in part II, we have included the factor $1/8\pi\mu$ in our expressions for G_{ij}^* and P_j^*. The boundary conditions to be applied at the surface of the slender body are,

$$\boldsymbol{u} = \boldsymbol{\omega} \wedge \boldsymbol{r},$$

or

$$u_\theta = \omega r_0(x_1), \quad u_r = u_x = 0 \tag{26}$$

in local cylindrical coordinates situated within the slender body.

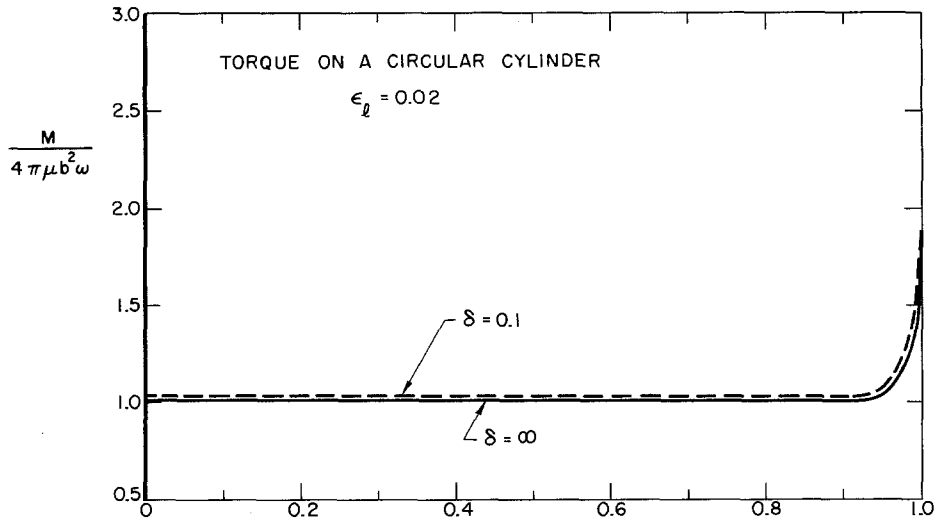

Figure 7. Graphs showing the numerical solutions for the torque on a rotating circular cylinder ($\varepsilon_l = 0.02$) for $\delta = 0.1$ and $\delta = \infty$ which corresponds to the infinite fluid case.

An extremely accurate approximate for the torque/unit length M_0 was obtained in equation (9). If we non-dimensionalise $M(x_1)$ with respect to M_0, we can obtain numerically (similar to the force) the results which are shown in Figure 7. A surprising result in the variation is only 1–2% from the infinite fluid ($\delta = \infty$) case for $\delta = 0.1$. However, on closer investigation of the integral equations we see that in an infinite fluid $M_0 \alpha \varepsilon_l^{-2}$ while the wall effect is $O(\delta^{-2})$ which in the case under consideration means the wall effect is two orders of magnitude less or around 1% as indicated above. That is, because of the rapid decay of the velocity, the wall effect is only significant when the slender body is very close to the wall.

6. Conclusions

The main aim in this paper is to obtain qualitative evidence of the influence of walls on the motion of micro-organisms. The wall effect can be increasing significant if the body approaches within a body length of the wall (e.g. coverslip or slide) and that motion towards the wall (F_3) is strongly discouraged. This indicates that it is quite plausible for planar motion to be induced in otherwise helical or three-dimensional beating patterns of flagella.

From the fluid mechanics viewpoint, the two most interesting features are (a) the ratio of normal to tangential resistance coefficients can be greater than two and (b) when the clearance from the wall is less than the length of the slender body, a much better order approximation to the drag is that of $O(1/\log(2h/R))$ where h is the height above the wall. Wall effects are insig-

nificant on an axially rotating slender body, within the confines of the above theory (i.e. the slender body is not too close to the wall), being about 1–2% off from the infinite fluid case.

Acknowledgements

This research was carried out under the joint support of the National Science Foundation, under Grant GK31161X and by the Office of Naval Research under contract N00014-67-A-0094-0012.

REFERENCES

[1] G. K. Batchelor, Slender body theory for particles of arbitrary cross-section in Stokes' flow, *J. Fluid Mech.*, 44 (1970) 419–440.
[2] J. R. Blake and A. T. Chwang, Singularities of viscous flow. Part I: The image systems in the vicinity of a stationary no-slip boundary, *J. Eng. Math.*, (to be published).
[3] J. M. Burgers, Second report on viscosity and plasticity. *Kon. Ned. Akad. Wet. Verhand.*, 16 (1938) 113–184.
[4] A. T. Chwang and T. Y. Wu, A note on the helical movements of micro-organisms, *Proc. Roy. Soc.*, B178 (1971) 327–346.
[5] A. T. Chwang and T. Y. Wu, Hydromechanics of low Reynolds number flows. Part I. Rotation of axisymmetric prolate bodies, *J. Fluid Mech.*, 1974 (submitted for publication).
[6] N. S. Clarke, The force distribution on a slender twisted particle in Stokes' flow, *J. Fluid Mech.*, 62 (1972) 781–793.
[7] R. G. Cox, The motion of long slender bodies in a viscous fluid. Part I. General Theory, *J. Fluid Mech.*, 44 (1970) 791–810.
[8] N. J. deMestre, Low Reynolds number fall of slender cylinders near boundaries, *J. Fluid Mech.*, 58 (1973) 641–656.
[9] J. Gray and G. J. Hancock, The propulsion of sea-urchin spermatozoa, *J. Exp. Biol.*, 32 (1955) 802–814.
[10] G. J. Hancock, The self propulsion of microscopic organisms through liquids, *Proc. Roy. Soc.*, A217 (1953) 96–121.
[11] H. Lamb, *Hydrodynamics* Cambridge University Press and Dover (1932).
[12] H. A. Lorentz, *Zittingsverlag. Akad. v. Wet.* (1896) 168–182.
[13] G. I. Taylor, Analysis of the swimming of long and narrow animals. *Proc. Roy. Soc.*, A214 (1952) 158–183.
[14] J. P. K. Tillett, Axial and transverse Stokes flow past slender axisymmetric bodies, *J. Fluid Mech.*, 44 (1970) 401–417.
[15] E. O. Tuck, Some methods for flows past blunt slender bodies, *J. Fluid Mech.*, 18 (1964) 619–635.
[16] E. O. Tuck, Toward the calculation and minimization of Stokes drag on bodies of arbitrary shape, *Proc. Aust. Conf. Hyd. Fluid Mech.*, 3 (1968) 29–32.
[17] H. Winet, Wall drag on free moving citated micro-organism, *J. Exp. Biol.*, 59 (1973) 753–766.